

Ultrasonic characterization of exhumed cast iron water pipes

Paul Groves, Giovanni Cascante*, and Mark Knight

Department of Civil and Environmental Engineering, University of Waterloo, Waterloo, ON, Canada N2L 3G1

(Received July 3, 2010, Accepted August 24, 2010)

Abstract. Cast iron pipe has been used as a water distribution technology in North America since the early nineteenth century. The first cast iron pipes were made of grey cast iron which was succeeded by ductile iron as a pipe material in the 1940s. These different iron alloys have significantly different microstructures which give rise to distinct mechanical properties. Insight into the non-destructive structural condition assessment of aging pipes can be advantageous in developing mitigation strategies for pipe failures. This paper examines the relationship between the small-strain and large-strain properties of exhumed cast iron water pipes. Nondestructive and destructive testing programs were performed on eight pipes varying in age from 40 to 130 years. The experimental program included microstructure evaluation and ultrasonic, tensile, and flexural testing. New applications of frequency domain analysis techniques including Fourier and wavelet transforms of ultrasonic pulse velocity measurements are presented. A low correlation between wave propagation and large-strain measurements was observed. However, the wave velocities were consistently different between ductile and grey cast iron pipes (14% to 18% difference); the ductile iron pipes showed the smaller variation in wave velocities. Thus, the variation of elastic properties for ductile iron was not enough to define a linear correlation because all the measurements were practically concentrated in single cluster of points. The cross-sectional areas of the specimens tested varied as a result of minor manufacturing defects and levels of corrosion. These variations affect the large strain testing results; but, surface defects have limited effect on wave velocities and may also contribute to the low correlations observed. Lamb waves are typically not considered in the evaluation of ultrasonic pulse velocity. However, Lamb waves were found to contribute significantly to the frequency content of the ultrasonic signals possibly resulting in the poor correlations observed. Therefore, correlations between wave velocities and large strain properties obtained using specimens manufactured in the laboratory must be used with caution in the condition assessment of aged water pipes especially for grey cast iron pipes.

Keywords: cast iron pipes; ductile iron pipes; ultrasonic; wave velocity; non-destructive evaluation.

1. Introduction

Grey cast iron pipes were used extensively in the construction of water distribution networks from the end of the nineteenth century until the late 1960s. Subsequently, the superior mechanical properties of ductile iron pipe became preferred. Throughout this period a variety of manufacturing technologies were used. As a result, cast iron pipes with varying compositions and ages exist today. Many of these pipes remain in service worldwide in old cities. For example, the average age of the water distribution system in the City of Toronto is 90 years. This network is comprised of approximately

*Corresponding Author, Dr., E-mail: gcascant@uwaterloo.ca

5347 km of predominantly small diameter (100 to 300 mm) cast iron piping. The occurrence of breaks in these aging pipes is estimated as 2 per week. (Seica and Packer 2004). With the increasing age and state of deterioration of cast iron pipes, an increase in the frequency of leaks and breaks can be expected to create more problems for water utility managers. Insight into the state of deterioration and structural condition of aging pipes can be advantageous in developing preventative and mitigation strategies for these frequent failures.

Nondestructive testing methods such as ultrasonic testing are commonly used for quality assessment of manufactured metals. Ultrasonic methods have been applied in wall thickness measurements for corrosion detection in cast iron pipes still in service (Skabo and Jackson 1991, Lee *et al.* 2008). Furthermore, relationships between ultrasonic velocity and microscopic properties of cast irons, such as percent carbon content, nodularity, and matrix composition, have been established in various studies (Tamburelli and Quaroni 1975, Orlowicz *et al.* 2010). The analysis of mechanical properties of exhumed cast iron pipes has been used in various studies to evaluate their state of deterioration (Rajani 2000, Seica and Packer 2004). These studies generally focus primarily on large strain mechanical properties such as tensile and flexural strength. They make limited use of ultrasonic testing for mapping corrosion through pipe thickness measurements.

Ohide *et al.* (1989) showed very good linear relationships between ultrasonic velocity and tensile strength among other mechanical properties for grey and ductile cast irons of varying grade. Samples of cast iron varied in amount of graphite and samples of ductile iron varied in amount of graphite and nodularity. Good linear relationships were observed between ultrasonic velocity and tensile strength for both grey and ductile irons when each different iron type was evaluated individually. The ductile samples had an average tensile strength about two times that of the grey cast iron samples and a greater standard deviation. In addition, the average ultrasonic velocity for the ductile samples was slightly greater than the average velocity of the grey iron samples. As a result, evaluating the relationship between velocity and strength for grey cast iron and ductile iron together does not give one trend but two linear relationships. Ohide *et al.* (1989) concluded that cast iron structure can be quantitatively assessed by measuring ultrasonic velocity provided that the manufacturing history of the iron is known.

Fuller *et al.* (1990) and Collins and Alchekh (1995) observed similar relationships between velocity and tensile strength for samples of ductile iron. Both these studies showed some non-linearity in the trends from samples with high velocity and strength. In all of the above mentioned studies, the manufacturing of the cast iron being tested is always carefully controlled and test specimens are machined with precise dimensions. In addition, not much consideration is given to frequency content of the ultrasonic energy or the impacts of specimen geometry on the results of ultrasonic testing.

This paper investigates the use of ultrasonic testing to provide insight into the structural integrity of exhumed cast iron water pipes. Non-destructive and destructive testing programs were performed on eight cast iron pipes ranging in service life from about 30 to 130 years. The pipes originated from different manufacturing materials and methods and had various diameters, wall thicknesses, and states of corrosion. The experimental program included microstructure examination, small strain measurements with ultrasonic testing and large strain measurements with tensile and flexural testing. The ultrasonic data analysis is performed not only in the time domain as traditionally done in ultrasonic testing but also in the frequency domain using the Fourier and the wavelet transforms (Camarata *et al.* 2010, Gokdag and Kopmaz 2010). The effect of Lamb wave propagation in the pipe samples on the recorded ultrasonic signals is evaluated. This kind of surface wave is rarely considered in the literature when presenting ultrasonic results. The relationship between the large

strain and small strain properties of cast iron used in water pipes is investigated.

This paper first provides some background information about cast iron and ultrasonic testing. Then the general methodology of the testing program is outlined and the experimental setup and methodology is explained. Next, the results of the microstructure evaluation and ultrasonic, tensile and flexural testing are presented. The analysis and discussion of these results follows. Finally, the conclusions of the study are presented.

Microstructure evaluation showed that three of the pipes were ductile iron and five of the pipes were grey cast iron. Ultrasonic pulse velocity and frequency content area, and tensile and flexural modulus, strength, and elongation were relatively higher in the ductile iron pipes than in the grey cast iron pipes. The ultrasonic velocity measurements on samples from an individual pipe did not correlate well with the corresponding large-strain properties. It is likely that the changes in microstructure between samples from the same pipe are not significant enough to be detected by the ultrasonic velocity measurements. Evaluations of changes in average ultrasonic velocities with average elastic moduli strengths and elongations between pipes do not show as good correlations as seen in the literature although similar trends were observed. Fourier analysis of the frequency content of the ultrasonic signals also did not find good correlations with large-strain parameters. Lamb waves were found to contribute significantly to the frequency content of the ultrasonic signals possibly contributing to the poor correlations. Daubechies's discrete wavelet transform was used in an attempt to isolate p-wave energy with shorter wavelengths and exclude the higher amplitude Lamb wave energy. The resulting analyses showed slight improvements in correlations between frequency spectra area and large strain measurements, but in general good correlations were still not observed. Although the literature shows good correlations between ultrasonic velocity and tensile strength in both grey cast iron and ductile iron, the specimens tested in these studies have regular and consistent geometries and changes in microstructure are carefully controlled through manufacturing processes. The samples tested in this study varied in cross-sectional area as a result of minor manufacturing defects and corrosion. These variations impact the large strain testing results but shallow surficial defects have limited effect on body wave velocity and may therefore contribute to the poor correlations observed throughout this study. This paper presents novel applications in the frequency domain analyses of ultrasonic pulse velocity measurements that have not been used in similar studies in the literature.

2. Cast iron

Cast iron pipe as a water distribution technology has been used in North America since the early nineteenth century (Koelble 2006). The first pipes were made of grey cast iron and manufactured using pit casting. This casting method was replaced by spin casting in the 1920s. This new manufacturing technique provided more even distribution of the molten iron during casting, reduction in the size of graphite flakes within the solidified microstructure and fewer manufacturing defects in general. Ductile iron succeeded grey cast iron as a pipe material in the 1940s. Pipes are currently made of ductile iron manufactured using spin casting and are commonly encased in polyethylene to mitigate corrosion (Seica and Packer 2004).

Cast iron is a generic term that applies to iron-carbon alloys containing more than two percent carbon; in general, it also contains small percentages of silicon and manganese, and trace amounts of phosphorous and sulphur. Cast iron unlike steel contains carbon in surplus of its solubility in

solid iron. The result of this excess carbon is the precipitation of crystalline graphite during freezing (Walton 1971). There is a variety of cast irons, including grey cast iron and ductile iron among others. Cast irons are generally classified by graphite shape and matrix composition. The microstructure of a cast metal depends primarily on chemical composition, cooling rate, and melt treatment (Davis 2006).

2.1 Grey cast iron

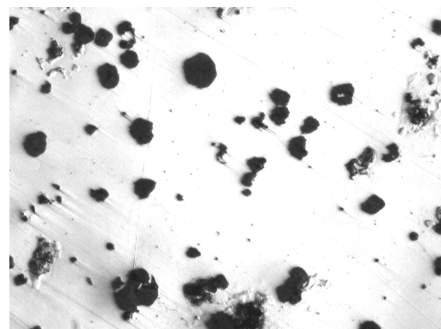
Grey cast iron has a characteristic grey colour which results from the graphite within the metal crystallized as flakes as seen in Fig. 1. The total carbon content of grey cast iron alloys generally ranges from 2.5 to 3.6%. The shape, size, amount, and distribution of the flakes vary between different grey cast irons. The cooling rate during the manufacture process has significant influence on flake morphology. Moderate cooling rates generally produce grey cast irons with the best mechanical properties (graphite flakes with uniform distribution and random orientation). The matrix of grey cast iron generally occurs in three common phases: ferrite, cementite, and pearlite. Ferrite is a softer phase consisting of nearly pure iron (low carbon content). Cementite is a harder phase composed of an intermetallic compound of iron and carbon. Pearlite is the most common matrix phase in grey cast irons and is characterized by lamellar plates of ferrite and cementite (Davis 2006).

2.2 Ductile iron

Ductile iron has higher ductility relative to other cast irons; it contains graphite in spheroidal nodules as seen in Fig. 1. This nodule formation is the result of certain additives (commonly magnesium) introduced to the molten iron during manufacturing. Their total carbon content generally ranges from 3.6 to 3.8% and the magnesium content from 0.03 to 0.06% (no magnesium in grey cast iron). The shape of the nodules can vary from flake form to true nodular form. Ductile iron commonly has more than 90% of the graphite in nodular form (90% nodularity). The size and uniformity of distribution also vary between different ductile irons. Spheroidal graphite is less affected by cooling rate than graphite flakes. The most common matrix phases in ductile irons are ferrite and pearlite or varying proportions of the two (Davis 1996).



Graphite flakes in gray cast iron



Graphite nodules in ductile iron

Fig. 1 Gray cast iron and ductile iron microstructures

Differences in physical and mechanical properties of cast irons arise from their varying microstructures. The shape of graphite in cast irons is the single most important factor affecting their mechanical properties. Typical values of elastic modulus, tensile strength, and elongation for grey cast irons are 65 to 160 GPa, 150 to 430 MPa, and 0.5 to 1.0%, respectively. Typical values of elastic modulus, tensile strength, and elongation for ductile irons are 170 to 175 GPa, 350 to 900 MPa, and 1.0 to 18.0%, respectively. The graphite flakes in grey cast iron act as stress concentrators; the sharpness of the graphite cavities increase internal stresses upon loading generating its characteristic brittle behaviour. These discontinuities are also responsible for the lower strength in grey cast iron relative to ductile iron. Increasing the carbon content increases the amount of graphite and thus reduces the strength of cast iron. Higher tensile strengths and elastic moduli are attributed smaller flakes. Furthermore, uniform as opposed to segregated flake distribution result in better mechanical properties (Davis 1996, Angus 1976). The matrix composition also affects the mechanical properties: ferrite has low strength and high ductility, cementite has high strength and brittle behaviour and pearlite has hardness and strength intermediary to those of ferrite and cementite, but higher to cementite with fine interlamellar spacing (Davis 2006).

The dispersion of graphite in ductile iron as spheroidal nodules increases the strength of the metal by up to seven times and dramatically improves ductility. All properties related to strength and ductility decrease as the proportion of non-nodular graphite within a ductile iron increases. The size and distribution of graphite nodules also affect the properties. Many small nodules tend to increase tensile properties. Excessive nodules may weaken a metal. As the amount of graphite in a metal increases, there is a relatively small decrease in the strength, modulus of elasticity and elongation. The matrix of ductile irons generally consists of varying proportions of ferrite and pearlite. The strength and hardness of an iron increases as the amount of pearlite increases (Davis 1996).

3. Ultrasonic testing

Ultrasonic testing uses the characteristics of the propagation of high frequency elastic waves ($f > 20$ kHz) through a media to evaluate its internal structure. The pulse velocity method is widely used for the assessment of the material wave velocity. In this method, a mechanical pulse is emitted by a transmitter, the pulse travels through the medium, and finally is detected by a receiver (Fig. 2). The travel time of the first arrival is precisely measured with electronic equipment. Typically, the transmitter and the receiver are placed on the opposite faces of the test object (Lu *et al.* 2010). The

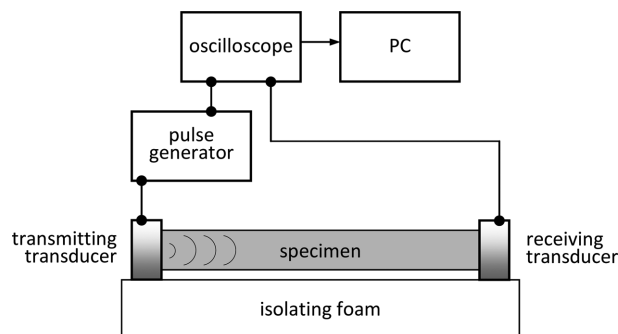


Fig. 2 Ultrasonic pulse velocity testing setup

first arrival time divided by the length of the sample gives a measure of the wave velocity (V). The velocity (V), frequency (f), and wavelength (λ) of any wave are related according to

$$v = f\lambda \quad (1)$$

Velocity is constant in a homogeneous medium. Primary waves (p-waves) are the fastest elastic waves and therefore are the first to be detected at the receiver when a pulse is initiated within a sample. The p-wave velocity (V_P) in a homogeneous medium is given by (Graff 1991).

$$V_P = \sqrt{\frac{M}{\rho}} \quad (2)$$

where M is the constrained modulus and ρ is the mass density of the material. The constrained modulus is related to the elastic modulus (E) and the Poisson's ratio (ν) according to

$$M = E \left[\frac{1 - \nu}{(1 + \nu)(1 - 2\nu)} \right] \quad (3)$$

Therefore, high wave velocities are attributed to stiff materials with high elastic moduli.

In a thin sample ($H \sim 1\lambda$, where H is thickness) Lamb waves are generated. These waves have symmetrical and anti-symmetrical mode shapes of propagation. The fundamental mode is the most important it spans all frequencies and carries more energy than higher modes (Blitz and Simpson 1996). Lamb waves are dispersive (different frequency components travel at different phase). The wave propagation of Lamb modes is governed by the Rayleigh-Lamb-frequency equation (Graff 1991)

$$\frac{\tanh(\beta h)}{\tanh(\alpha h)} + \left[\frac{4\alpha\beta k^2}{(\beta^2 - k^2)^2} \right]^{\pm 1} = 0 \quad (4)$$

$$\alpha^2 = k^2 - \frac{\omega^2}{V_P^2} \quad \beta^2 = k^2 - \frac{\omega^2}{V_S^2} \quad k = \frac{\omega}{V_{ph}}$$

where V_P and V_S are the P -wave and secondary wave velocities, respectively; ω is the angular frequency; k is the wave number; V_{ph} is the phase velocity; h is half the thickness of a plate. The exponent +1 represents the solution for the symmetric Lamb modes; while the exponent -1 represents the solution for the anti-symmetric Lamb modes. With respect to a plane at the middle thickness of a plate, symmetric Lamb modes generate waves with symmetric thickness variation, and anti-symmetric Lamb modes generate waves with anti-symmetric thickness variation.

For a typical cast iron plate ($V_P=5500$ m/s, $V_S=2800$ m/s, and $h=4$ mm) the dispersion curves for Lamb modes are calculated in Fig. 3 using Eq. 4. Fundamental modes S0 and A0 show dispersion at low frequencies. Their phase velocities converge to the Rayleigh wave velocity at higher frequencies where $\lambda \sim h$. Higher Lamb modes appear at sequentially higher resonant frequencies. The fundamental mode Lamb waves create significantly larger movements at the surface of a medium than p-waves and can therefore mask the p-wave energy arriving at a specific point. Lamb wave arrivals can be mistaken for p-wave arrivals if adequate resolution is not used in data acquisition therefore affecting the reported velocity.

Commonly, only the arrival time is analyzed in the pulse velocity test; which represents a single data point in the time domain. Conversely, Fourier analysis can be used to access information contained

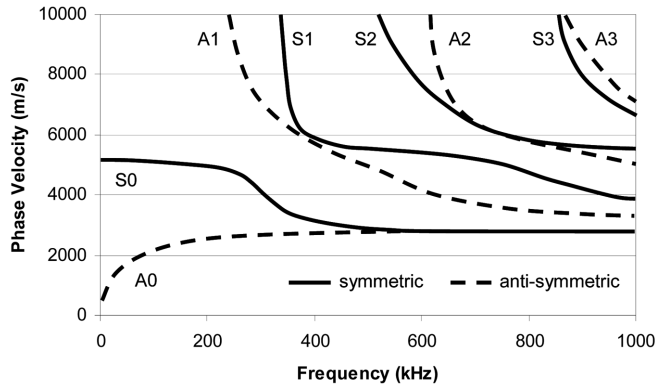


Fig. 3 Theoretical dispersion curves for a typical cast iron plate ($V_p = 5500$ m/s, $V_s = 2800$ m/s, and $h = 4$ mm)

within the frequency content of the entire signal. The discrete Fourier transform, $X(f)$, of the time domain signal, $x(t)$, is given by (Bracewell 2007).

$$X(f) = \sum_t x(t) \cdot e^{-i(2\pi f)t} \quad (5)$$

where t is time ($t=j\Delta t$), f is frequency ($f=k\Delta f$), Δt and Δf are the discrete steps in time and frequency, j and k are integer indices or counters, and i is the imaginary unit ($i^2 = -1$). Each component of the frequency spectrum $X(f)$ represents the relative participation of a sinusoidal function with frequency f in the measured signal. The Fourier transform gives information about the frequency content but does not give information about the location of these frequencies in the time domain.

The wavelet transform (WT) provides a significant advantage over Fourier transforms: the ability to see changes in frequency content with time. These functions decompose the original signal into its different frequency components. Daubechies' Wavelets are one of the most commonly used discrete WTs. This WT decomposes the original signal into coefficients representing the energy within the signal at different frequencies. The coefficients within different levels of frequency bandwidth are used to reconstruct time signals at these different levels (eg., 0 to 1 kHz, 1 to 3 kHz, ..., 500 to 1000 kHz). The number of levels and their frequency bandwidth is dictated by the sampling rate and the length of the signal. These new time signals describe the changes specific frequency bandwidths occurring in the time domain.

The wave velocity (V) and frequency content of an ultrasonic signal allow the calculation of the wavelengths (λ) generated during testing (Eq. 1). Generally, ultrasonic tests are able to resolve features of one wavelength and greater in size. Furthermore, if the wavelengths are large in comparison with the length of the specimen, the measured velocity is incorrect. The wavelengths should be at least half the length of the specimen to avoid near-field effects (Graff 1991). Thus, the evaluation of the wavelengths generated is critical to ensure the validity of the results.

The area of the frequency spectrum is an indication of the energy of the signal. Waveform energy is inversely proportional to frequency. As a result, high frequencies attenuate faster than low frequencies as a wave travels through a medium. Different materials have different damping properties and will therefore attenuate elastic energy to greater or lesser extents. Generally, materials with more defects have greater attenuating effects than sound materials. This relationship between pulse energy and frequency influences the selection of source frequency content and consequently also the resolution

Table 1 Tested pipe sections

| Pipe ID | Pipe diam. (in.) | Manuf. year | Service location | Avg. wall thickness | | Avg corros. thickness | | Comments |
|---------|------------------|-------------|------------------|---------------------|-----------------|-----------------------|-----------------|--------------------|
| | | | | (mm) | CV ¹ | (mm) | CV ¹ | |
| 4A | 4 | 1962 | North Bay, ON | 7.6 | 2% | none | | inner cement liner |
| 4B | 4 | 1962 | North Bay, ON | 10.2 | 3% | 2.4 | 40% | - |
| 4C | 4 | 1975 | North Bay, ON | 10.5 | 5% | none | | - |
| 6A | 6 | 1970 | North Bay, ON | 9.0 | 10% | 1.0 ² | 46% | inner cement liner |
| 12A | 12 | 1976 | North Bay, ON | 6.6 | 9% | none | | inner cement liner |
| 18A | 18 | 1860 | Hamilton, ON | 16.1 | 13% | 2.7 | 74% | - |
| 18B | 18 | 1860 | Hamilton, ON | 16.5 | 7% | 1.2 | 114% | - |
| 18C | 18 | 1860 | Hamilton, ON | 20.3 | 2% | 2.8 | 35% | - |

¹Coefficient of variance

²Corrosion here refers to discolouration observed inside cement liner

of the test. A high-frequency source may not be practical in a high-attenuating material. The energy of the source pulse may be dissipated before it reaches the receiver depending on the source-receiver separation distance (Yang *et al.* 2009).

4. Experimental methodology

A laboratory-testing program was designed to measure the small strain and large strain properties of eight sections of exhumed cast iron pipes. The measurement of small strain parameters involved ultrasonic pulse velocity testing. The large strain measurements included tensile testing and flexural testing. A summary of the pipe sections tested is presented in Table 1. The wall thickness and relative conditions varied between the pipes. Average pipe-wall thickness and corrosion depth for each pipe is presented in Table 1. The sections of pipe varied in length from 47 to 110 cm. These sections were first cut into lengthwise strips. Ultrasonic measurements were done on these initial full-length strips. Smaller coupons (about 20 cm length) were cut longitudinally from these strips with a water jet for the various lab tests. Representative samples were prepared and examined with an optical microscope to evaluate microstructure. Ultrasonic measurements were also performed on all the 20-cm coupons before the large-strain testing. Measurements on each coupon permitted the observation of changes in wave properties and large-strain properties within individual pipes and allowed for the assessment of any correlations between these measured parameters. Tensile testing was performed on coupons from all pipes while flexural testing was done on samples from only pipes 4A, 4B, 4C, 6A and 12A. Flexural testing was not performed on the 18-inch pipes because of a limited amount of material available.

5. Experimental setup and testing procedures

5.1 Microstructure evaluation

Representative samples from each pipe were polished and digitally photographed at varying levels of magnification. A general assessment of the microstructure of the pipes was required, thus the ASTM

procedures for preparing metal samples for microstructure analysis were followed only partially. Consequently, some striations are visible in the microstructure pictures presented in later sections.

5.2 Ultrasonic pulse velocity test

Ultrasonic testing was conducted on all samples cut for the tensile and flexural testing. The dimensions of these samples are presented in the following sections. The instrumentation used for ultrasonic testing consists of two compressional-wave (p-wave) piezoelectric transducers (1 MHz, Panametrics V102-RM), a pulse generator (Panametric Pulser Receiver Model 5052PR), a digital oscilloscope (HP 54610B), a sample mounting frame, a load cell (type 50 DBB, capacity 500 N), a power supply (HP 3620 A), a digital multimeter (HP 34401 A), and a computer. For each test, a sample was mounted between the two transducers on the frame equipped with the load cell. Vacuum grease was used as ultrasonic couplant between sample and transducers. The load cell output was monitored with the digital multimeter to measure the pressure applied on the transducers. A constant pressure of about 150 kPa was maintained in all tests to improve the repeatability of the results.

The travel time between the transducers was measured with the digital oscilloscope (resolution $\Delta t = 0.01 \mu\text{s}$). The p-wave velocity was determined by dividing the sample length by the travel time. The complete time history of the arriving wave was transferred to the computer using a GPIB interface (resolution $\Delta t = 0.1 \mu\text{s}$) for later signal processing. The ultrasonic equipment was calibrated by measuring the travel time on a series of steel samples of different length following the procedure suggested by Khan *et al.* (2010). The measured arrival times are plotted against the corresponding sample length and a line of best fit is evaluated. The line intercept represents the inherent time delay for the system ($0.4 \mu\text{s}$) which is subtracted from all the arrival times recorded in this study.

5.3 Tensile test

Tensile tests were performed following to the ASTM standard E8 (ASTM E8/E8M-08 2008). Tensile coupons were cut according to the sheet-type, ½-in wide specifications. These dogbone-shaped samples were 20 cm long with a reduced section of 1.3 cm width, and grip sections on either side of 5.7 cm long. The thicknesses of the coupons were the same as the wall-thickness of the original pipe. Some coupons required machining to provide flat gripping areas to prevent breakage at the hydraulic grips. The testing equipment included a hydraulic load frame and hydraulic grips (MTS Model 322 for 18 in diameter pipes, MTS Model 810 for other pipes), a digital extensometer (MTS Model 634.25E-24 with 2 in gage length), and a data acquisition system. All tensile testing was performed at a constant strain rate of 0.5 mm/min. The coupons were loaded until failure. Force data from the MTS machines and displacement data from the extensometer were transferred to the computer for later analysis.

5.4 Flexural test

Flexural tests were performed following the ASTM standard D790. (ASTM D790-07 2007). The flexural samples were 22 cm long by 2.5 cm wide to accommodate the required span length and width. The thicknesses of the coupons were the same as the wall-thickness of the original pipe section. The samples were tested on a hydraulic load frame (MTS Model 810) equipped with curved loading noses and supports which are changed to match the outer and inner curvatures of the

different pipes. The samples are loaded to failure at a constant strain rate of 5 mm/min. Force and displacement data from the MTS machine is transferred to the computer for later analysis.

6. Results

6.1 Microstructure evaluation

Fig. 4 presents pictures of the polished cast iron samples at $50\times$ magnification. Only one sample was taken to represent the 18 in diameter pipes as these were all made around the same time and at the same foundry. Table 2 summarizes some general observations on the different microstructures presented above.

6.2 Ultrasonic pulse velocity testing

A typical time signal and the average frequency spectrum (average of all coupons from each pipe) from each pipe are presented in Figs. 5 and 6, respectively. The average p-wave velocity measurement from the long strips and from the short coupons for each pipe is presented in Table 3.

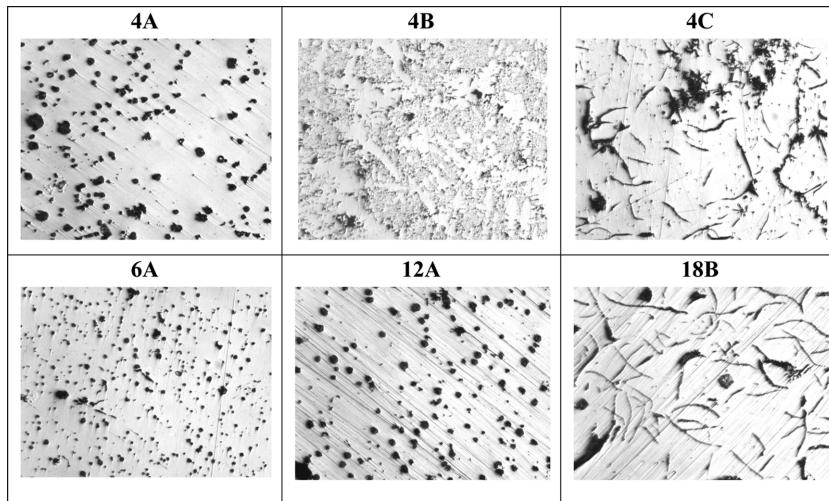


Fig. 4 Pictures of pipe microstructures ($50\times$ magnification)

Table 2 Microstructure general observations

| Pipe No. | Graphite shape | Distribution | Relative size | Type of cast iron |
|----------|----------------|--------------|---------------|-------------------|
| 4A | Nodules | Uniform | Large | Ductile |
| 4B | Flakes | Segregated | Very Short | Grey |
| 4C | Flakes | Uniform | Long | Grey |
| 6A | Nodules | Uniform | Small | Ductile |
| 12A | Nodules | Uniform | Large | Ductile |
| 18B | Flakes | Uniform | Long | Grey |

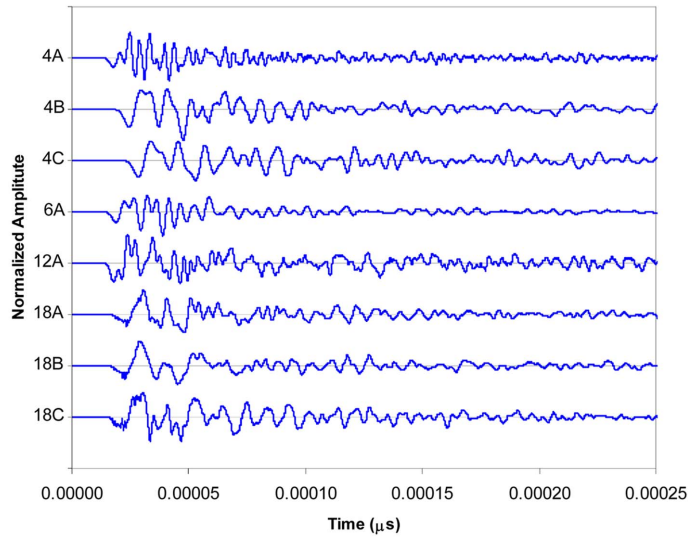


Fig. 5 Typical time signals

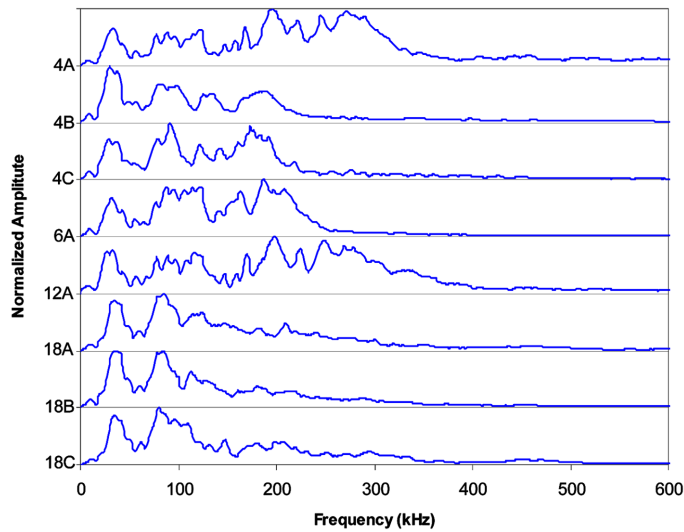


Fig. 6 Average frequency spectra

6.3 Tensile testing

Typical tensile stress-strain curves from each pipe are illustrated in Fig. 7. The large strain parameters obtained from the tensile testing included the tensile strength and the elongation. Tensile strength was taken as the maximum stress sustained by the test specimen while the elongation was measured as the strain at this maximum stress. The elastic modulus was measured from the initial tangent to the stress-strain curve (about 0.01 to 0.05% strain). A summary of the parameters obtained from the tensile testing are presented in Table 4.

Table 3 P-wave velocity (V_p) measurements

| Pipe ID | Strips | | | Coupons | | |
|---------|-------------|-----------|------|-------------|-----------|------|
| | Length (cm) | Avg V_p | | Length (cm) | Avg V_p | |
| | | (m/s) | CV | | (m/s) | CV |
| 4A | 103.9 | 5195 | 0.4% | 22.0 | 5545 | 0.3% |
| 4B | 81.1 | 4655 | 0.8% | 22.0 | 4966 | 0.2% |
| 4C | 47.3 | 4642 | 1.1% | 22.0 | 4743 | 2.9% |
| 6A | 109.8 | 5211 | 0.8% | 22.0 | 5514 | 0.7% |
| 12A | 98.7 | 5223 | 0.7% | 22.0 | 5549 | 0.9% |
| 18A | - | - | - | 20.0 | 4776 | 0.9% |
| 18B | - | - | - | 20.0 | 4892 | 1.3% |
| 18C | - | - | - | 20.0 | 4898 | 0.7% |

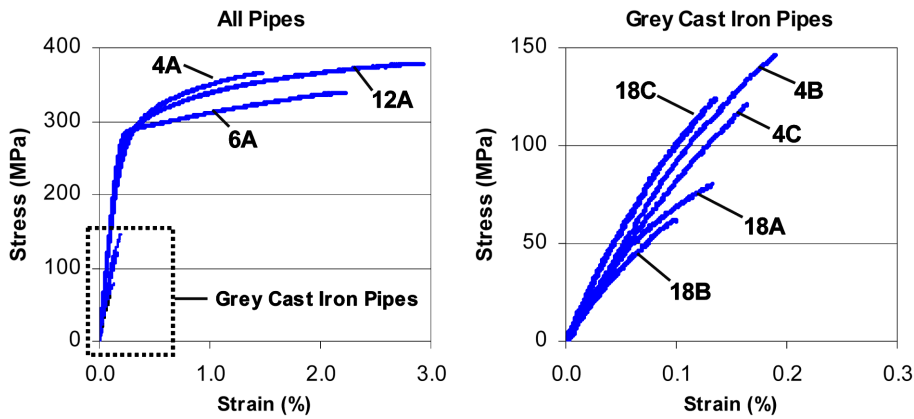


Fig. 7 Typical tensile stress-strain curves

Table 4 Tensile testing results

| Pipe ID | No. of coupons tested | Avg. Elastic modulus | | Avg. Tensile strength | | Avg. Elongation | |
|---------|-----------------------|----------------------|-----|-----------------------|-----|-----------------|-----|
| | | (MPa) | CV | (MPa) | CV | (%) | CV |
| 4A | 12 | 153093 | 3% | 356.6 | 5% | 1.7 | 30% |
| 4B | 8 | 97856 | 10% | 144.7 | 11% | 0.2 | 13% |
| 4C | 3 | 88543 | 7% | 121.5 | 9% | 0.2 | 16% |
| 6A | 8 | 160091 | 7% | 317.6 | 13% | 2.2 | 29% |
| 12A | 9 | 150667 | 9% | 334.5 | 12% | 2.3 | 33% |
| 18A | 8 | 88921 | 9% | 63.2 | 35% | 0.1 | 42% |
| 18B | 5 | 91900 | 17% | 76.4 | 22% | 0.1 | 30% |
| 18C | 10 | 110028 | 13% | 122.0 | 30% | 0.2 | 48% |

6.4 Flexural testing

Typical flexural stress-strain curves from each pipe are illustrated in Fig. 8. The large strain parameters obtained from the flexural testing included the flexural strength and the flexural

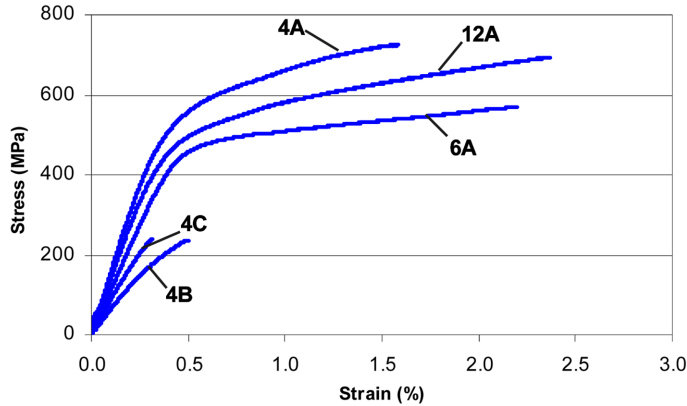


Fig. 8 Typical flexural stress-strain curves

Table 5 Flexural testing results

| Pipe ID | No. of coupons tested | Avg. Flexural modulus | | Avg. Flexural strength | | Avg. Flexural elongation | |
|---------|-----------------------|-----------------------|-----|------------------------|-----|--------------------------|-----|
| | | (MPa) | CV | (MPa) | CV | (%) | CV |
| 4A | 4 | 147573 | 7% | 697.6 | 9% | 1.57 | 8% |
| 4B | 4 | 64825 | 19% | 253.3 | 14% | 0.54 | 9% |
| 4C | 4 | 74474 | 12% | 241.8 | 14% | 0.41 | 17% |
| 6A | 4 | 128964 | 10% | 622.5 | 7% | 2.15 | 17% |
| 12A | 8 | 133601 | 17% | 669.7 | 15% | 2.22 | 15% |

elongation. Flexural strength was taken as the maximum stress sustained by the test specimen while the flexural elongation was measured as the strain at this maximum stress. The flexural modulus was measured from the initial tangent to the stress-strain curve (about 0.10 to 0.15% strain). A summary of the parameters obtained from the flexural testing are presented in Table 5.

7. Analysis and discussion

The correlations between the small-strain measurements from ultrasonic testing and the large-strain measurements from tensile and flexural testing are investigated. The Pearson product moment correlation coefficient ($-1 < r < 1$) is used to evaluate the linear relationship between various combinations of data sets. Abdel-Megeed suggests that five or more data points are required for accurate correlation coefficients (1984). The Pearson coefficient was preferred to the coefficient of determination (R^2) because it reflects the positive or negative nature of the linear trend in the data and the degree of correlation. Positive linear relationships between ultrasonic velocity and tensile have been established in the literature. Therefore positive correlations are expected between the ultrasonic wave properties and large-strain measurements examined in this study. For the purposes of this paper, an r value of +0.6 or above is considered to indicate a relationship with reasonable correlation between data sets because of the inherent variability in the pipe samples (variation in pipe wall thickness and corrosion depths as seen in Table 1).

7.1 Correlation of p-wave velocity with large strain parameters

A significant increase in average V_p measurements (up to 350 m/s) from the long strips to the short coupons is observed in Table 3. This change in velocity illustrates the effect of sample dimension on ultrasonic velocity measurements. The time measured in an ultrasonic velocity test originates from the arrival of the high frequency p-wave. A longer sample attenuates ultrasonic energy, especially higher frequencies, to a greater extent in comparison to a shorter sample because of the larger travel time. An attenuated p-wave arrival can be missed or not seen at all depending on the resolution of the testing equipment. As a result, the later arrival of s-waves or surface waves is measured therefore reporting a slower velocity.

The relationships between the p-wave velocity of each coupon from an individual pipe and the corresponding elastic modulus, tensile strength, tensile elongation, flexural modulus, flexural strength, and flexural elongation were evaluated. The r values calculated for the correlations between the p-wave velocity and these large-strain parameters are presented in Table 6. To give an appreciation for the data dispersion associated with specific r values, various correlations of p-wave velocity and elastic modulus are shown in Fig. 9.

Table 6 Correlation coefficients (r) for coupon p-wave velocity (V_p) versus large-strain parameters

| Pipe ID | r for Tensile testing measurements | | | r for Flexural testing measurements | | | | |
|---------|--------------------------------------|----------------|-----------------|---------------------------------------|----------------|----------------|-----------------|---------------|
| | No. of amples | VP vs. Modulus | VP vs. Strength | VP vs. Elong. | No. of Samples | VP vs. Modulus | VP vs. Strength | VP vs. Elong. |
| 4A | 12 | 0.11 | -0.07 | 0.25 | 4 | -0.64 | -0.11 | -0.25 |
| 4B | 8 | 0.25 | 0.43 | 0.14 | 4 | 0.47 | 0.23 | -0.47 |
| 4C | 3 | 0.31 | 0.55 | 1.00 | 4 | 0.92 | -0.03 | -0.81 |
| 6A | 8 | 0.23 | -0.06 | -0.30 | 4 | 0.46 | 0.81 | 0.66 |
| 12A | 9 | 0.64 | 0.74 | 0.01 | 8 | 0.31 | 0.30 | 0.17 |
| 18A | 8 | 0.09 | -0.37 | -0.40 | - | - | - | - |
| 18B | 5 | 0.97 | 0.18 | -0.75 | - | - | - | - |
| 18C | 10 | 0.20 | 0.41 | 0.41 | - | - | - | - |

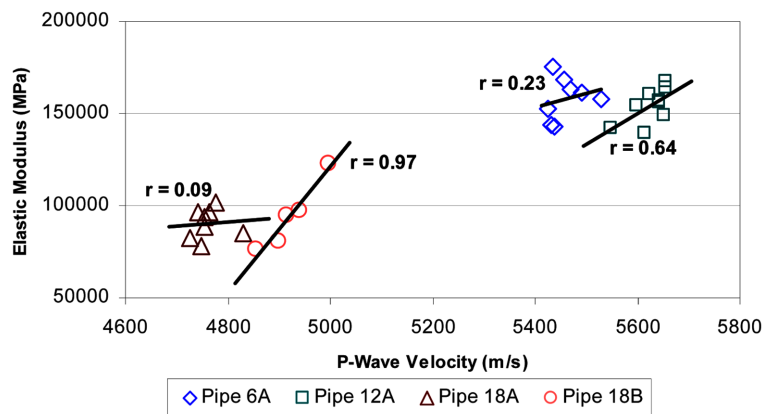


Fig. 9 Various r values from p-wave velocity and elastic modulus relationships (r related to scatter of points not trend-slope)

In general, the p-wave velocity and the large-strain parameters are not well correlated. Only 5 of the 39 comparisons presented in Table 6 have r values greater than 0.6. This lack of correlation may be caused by the variation in cross-sectional area due to manufacturing defects and corrosion observed in the coupons. The velocity of p-waves traveling through the body of a coupon will not be significantly impacted by shallow defects. However, reductions in cross-sectional area will affect the large stress and strain behaviour of the coupons. In addition, limited variation in carbon content and other microscopic properties between coupons may not be significant enough to be captured by the p-wave velocity. At a frequency of 1.0 MHz with an approximate velocity of 5000 m/s the corresponding wavelength is 5 mm. The differences in microstructure between different coupons from one pipe are at least an order magnitude smaller than half this wavelength. Using a higher frequency source could improve such correlations. Higher frequencies will generate smaller wavelengths and therefore increase the resolution of the testing. However, depth of penetration and therefore length of sample are reduced with increased source frequency.

Better correlations of p-wave velocity with both moduli are observed than with the strengths and elongations. The ultimate strength and strain at failure are affected by cracks or corrosion that act as stress concentrators at the surfaces samples. As previously mentioned, p-waves velocity is not sensitive to shallow surficial defects. Considering the above mentioned and that the tensile modulus and flexural modulus were measured at lower strain levels (0.01 to 0.05% and 0.05 to 0.10% respectively) better correlation between the p-wave velocity and the moduli is expected than with strength and elongation.

With the exception of pipes 4A and 12A, the correlation of the p-wave velocity with the flexural modulus was generally than with the tensile modulus. A more accurate extensometer was used in the tensile testing and therefore better correlations with the tensile data were expected. Less data points in these flexural comparisons (only four coupons) than in most of the tensile comparisons may contribute to these higher r values.

Average values of velocity and large strain parameters from all tested coupons were used to evaluate global correlations between pipes. Correlations of average velocity with average elastic modulus, tensile strength, and elongation for each pipe are presented in Figs. 15(a), (b), and (c), respectively. The average is computed from the measured parameters from all coupons from one pipe. Two distinct groups of data points are seen in these figures: the ductile iron pipes have higher p-wave velocities and large strain parameters than the grey cast iron pipes. Fig. 15 shows error bars indicating one standard deviation for velocity, modulus, strength and elongation measurements. The velocity measurements had significantly smaller standard deviations than the large strain measurements (in some cases, error bars are not seen in Fig. 15 because these are smaller than the data points). The velocity measurements show less scatter because they originate from very precise measurements of length and time while the stress and strain measurements were more influenced by the varying conditions of the coupons (geometry, thickness, and corrossions depth varies between coupons).

The literature has shown very good positive linear relationships between ultrasonic velocity and tensile strength in both grey cast irons and ductile irons. However, in these studies the specimens tested are carefully machined with uniform geometries. In addition, significant changes in microstructure (eg., matrix composition, percent carbon, nodularity) are induced through planned changes in the chemical composition and manufacturing process. Such successful correlations are not observed in Fig. 15. These poor relationships between ultrasonic velocity and the large strain parameters may be again caused by effects of variations in pipe condition. Futhermore, the changes in microstructure between pipes may not be as significant as the changes in manufactured samples used in other

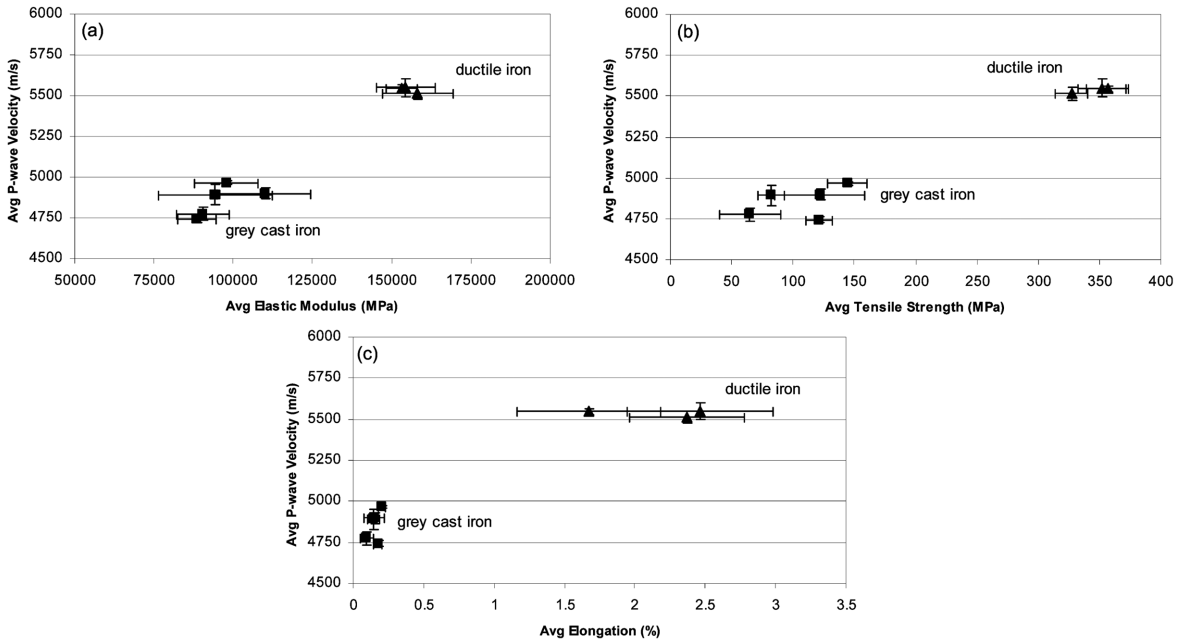


Fig. 10 Relationships between average p-wave velocity and: (a) elastic modulus, (b) tensile strength, (c) elongation

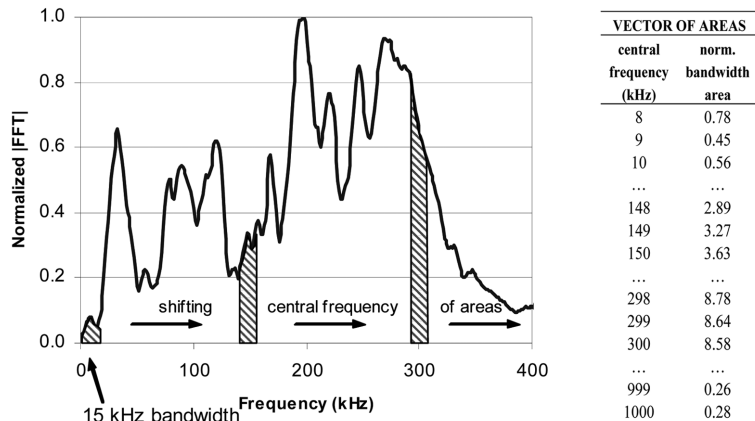


Fig. 11 Illustration of shifting bandwidth areas in |FFT| frequency spectra from coupon 4A01

studies. The large strain parameters presented in Fig. 15 do show the expected increase with p-wave velocity measurements for the brittle pipes but with significant scatter in the data points. Only the velocity and tensile strength showed a positive relationship in the ductile irons while elastic modulus and elongation decreased slightly with velocity. Specific r values were not evaluated for the global correlations because of the limited number of data points.

7.2 Correlation of frequency content with large strain parameters

The frequency contents of the recorded ultrasonic signals were used as an indication of attenuation. It was hypothesized that samples with lower large-strain values would cause greater

attenuation of the ultrasonic signals and that the frequency spectra would be more sensitive to these changes than the velocity measurements. The relationship between the total area of the FFT magnitude (|FFT|) frequency spectrum measured from each coupon in an individual pipe with the corresponding elastic modulus was evaluated. These showed low correlation.

An algorithm was developed to examine correlations between specific areas within the |FFT| frequency spectra and the elastic moduli from each coupon for individual pipes. Five different areas with specific frequency bandwidths (15 kHz, 35 kHz, 40 kHz, 55 kHz, and 100 kHz) were selected based on the peaks and other areas of significant energy observed in the frequency spectra. For the spectrum from an individual coupon, the algorithm shifts the central frequency of the first bandwidth area from 0 to 1 MHz. The result is a vector with a value of the bandwidth area at each corresponding central frequency (Fig. 11). This process is repeated to generate a vector of areas for each coupon from the same pipe. A correlation coefficient is then obtained for the relationship between the bandwidth area from each coupon spectrum at a specific central frequency and the elastic modulus of each coupon (Fig. 12). A vector containing the change in correlation coefficient with area at different central frequencies is then plotted to show if good correlations exist and at what frequencies the best correlations occur (Fig. 13). The process is repeated for the remaining frequency bandwidths which produced five vectors of correlation coefficient changing with central frequency (Fig. 14).

The algorithm was first used to evaluate the correlation between the unaltered frequency spectra

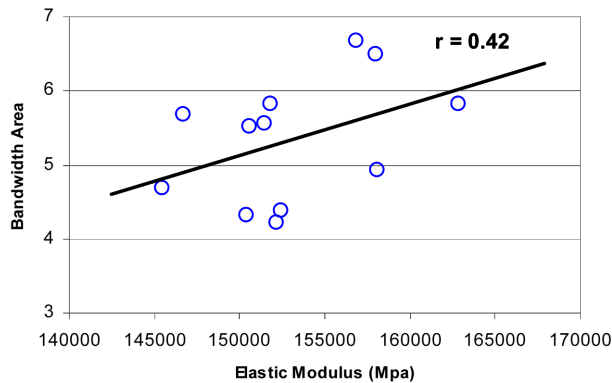


Fig. 12 Correlation coefficient (r) from 15 kHz bandwidth area centred at 168 kHz

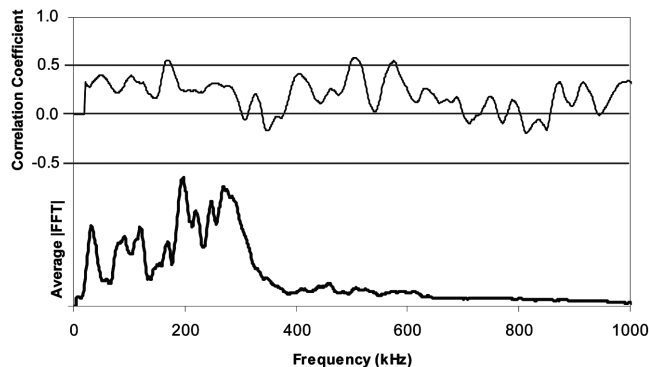


Fig. 13 Correlation coefficient from 15 kHz bandwidth area plotted with average |FFT| of all coupons in 4A

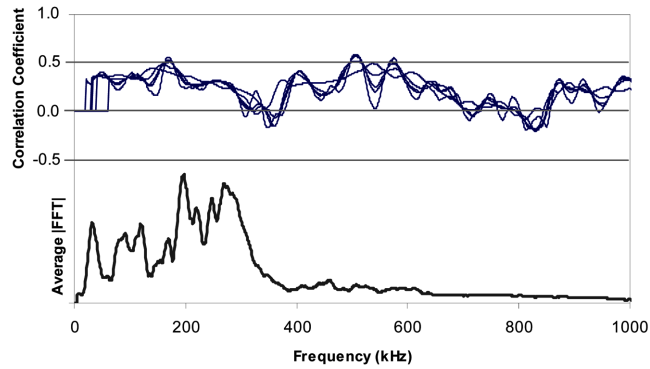


Fig. 14 Correlation coefficients from all bandwidth (15, 35, 40, 55, and 100 kHz) areas plotted with average |FFT| of all coupons in 4A

collected during the ultrasonic testing and the elastic moduli from each individual coupon for all pipes. The reported correlation coefficient for each pipe was taken from the maximum peak where the 15, 35, and 45 kHz r curves converged (eg. peak in r curves at about 510 kHz in Fig. 14). The 55 kHz and 100 kHz bandwidths were too wide to show any good correlations. The resulting r values are presented in Table 7. Good correlations were only observed in three of the pipes (4B, 12A, 18A). Various combinations of normalizing in both the time and frequency domains were attempted to remove any coupling effects from the |FFT| spectra. The best results came from normalizing each time signal to its maximum prior to performing the FFT. The resulting r values are shown in Table 7. The normalization improved the r values slightly for five pipes (4B, 4C, 6A, 18B, and 18C) and reduced r values for the remaining pipes (4A, 12A, 18A).

It is likely that better correlations between the frequency spectrum areas and E were not obtained because of interference by Lamb wave energy. This type of wave is rarely considered in ultrasonic studies presented in the literature. Lamb wave dispersion curves were generated for each pipe according to Eq. 4 to determine what ranges of the frequency spectra might originate from Lamb

Table 7 Maximum correlation coefficients (r) for coupon frequency spectrum bandwidth areas (A) versus elastic modulus (E)

| Pipe ID | No. of samples | r for Bandwidth area vs. Elastic modulus | | | | |
|---------|----------------|--|-----------------------|--------------------|--------------------------|--------------------|
| | | FFT Spectra areas | | | WT Spectra areas | |
| | | Freq. ¹ (kHz) | No Norm. ² | Norm. ³ | Freq. ¹ (kHz) | Norm. ³ |
| 4A | 12 | 509 | 0.59 | 0.46 | 505 | 0.71 |
| 4B | 8 | 610 | 0.66 | 0.67 | 660 | 0.82 |
| 4C | 3 | 865 | 0.33 | 0.93 | 500 | 0.92 |
| 6A | 8 | 450 | 0.36 | 0.52 | 550 | 0.48 |
| 12A | 9 | 460 | 0.70 | 0.68 | 250 | 0.49 |
| 18A | 8 | 490 | 0.88 | 0.85 | 500 | 0.86 |
| 18B | 5 | 745 | 0.47 | 0.66 | 250 | 0.73 |
| 18C | 10 | 365 | 0.42 | 0.54 | 450 | 0.57 |

¹Central frequency of area with maximum correlation

²Time signals and frequency spectra un-altered

³Time signals normalized to remove coupling effects

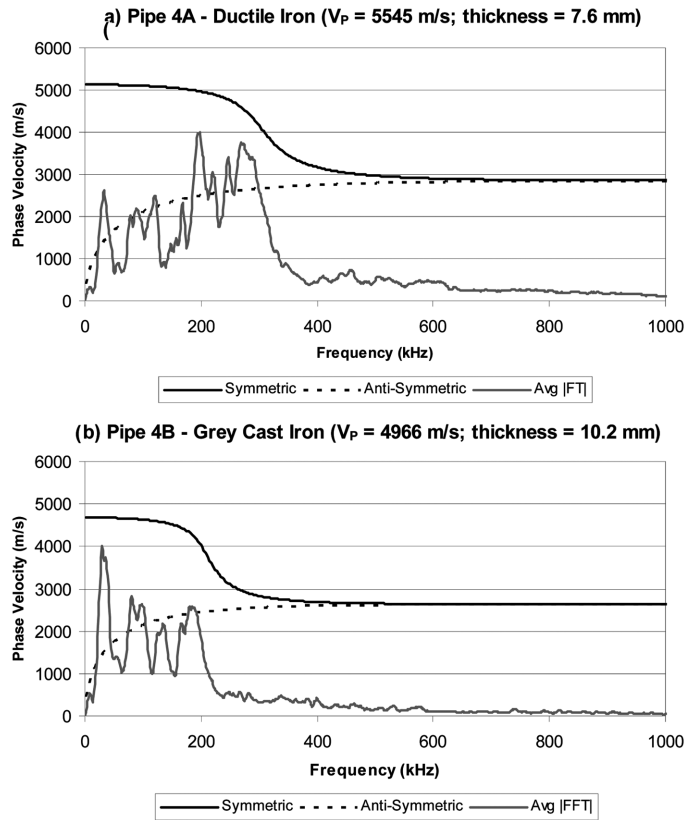


Fig. 15 Lamb mode dispersion curves for: (a) pipe 4A and (b) pipe 4B

waves. The average p-wave velocity and average thickness of each pipe were used in the calculations. Typical dispersion curves for ductile iron and grey cast iron are presented in Figs. 15(a) and (b), respectively. Both the symmetric and anti-symmetric fundamental modes are plotted. The dispersion curves showed that the main frequency content from the time signals measured in all the pipes occurs in the dispersive frequency range for Lamb waves. Fig. 12 shows that the average frequency spectra have main peaks in the lower frequency range where the symmetric and anti-symmetric mode phase velocities are changing with frequency (below 400 kHz in Fig. 15(a) and below 250 kHz in Fig. 15(b)). Lamb waves are geometrically dispersive; the dispersive range of frequencies depends mainly on the thickness of the sample. Thus, changes in the sample geometry generate variations in the measured wave velocities that are not related to differences in material properties.

The Wavelet transform was used to isolate p-wave energy with shorter wavelengths and exclude the higher amplitude Lamb wave energy especially in the lower frequency range. To the knowledge of the authors of this paper, this approach has not previously been applied to ultrasonic testing data for cast irons. Debauchies' discrete wavelet transform (DDWT) was used to decompose the time signals into different frequency levels. Fig. 13 presents an example of a decomposed signal. Reconstructed time signals from each coupon from 1000, 500, 250, 125, and 62.5 kHz levels were extracted. Each signal was again normalized in the time domain and FFTs were completed. These frequency spectra were then analyzed using the shifting area algorithm. The best correlations came

from the 500 kHz level time signals supporting the theory that the lower frequency Lamb waves do not show good correlation with material properties. The resulting r values are presented in Table 7. The wavelet analysis improved the r values for three pipes (4A, 4B, and 18B), reduced the r value for two pipes (6A and 12A) while the remaining r values changed very little in comparison to the original Fourier area comparison. Relationships between frequency spectra area and tensile strength and elongation were not completed because better correlations with these large-strain parameters controlled by surface defects than with relatively lower strain elastic moduli were not expected. The final results of the wavelet analysis showed improved correlations from the velocity analysis but still not consistent relationships between frequency spectrum areas and elastic modulus.

8. Conclusions

This paper examines the relationship between the small-strain and large-strain properties of exhumed cast iron water pipes. Non-destructive and destructive testing programs were performed on eight pipes varying in age from 40 to 130 years. Microstructure evaluation showed that three of the pipes were ductile iron and five of the pipes were grey cast iron. Ultrasonic pulse velocity and frequency content area, and tensile and flexural modulus, strength, and elongation were relatively higher in the ductile iron pipes than in the grey cast iron pipes.

The ultrasonic wave velocity measurements on samples from an individual pipe were not well correlated with the corresponding large-strain properties. However, wave velocities were consistently different between ductile and grey cast iron pipes (14% to 18% difference); the ductile iron pipes showed the smaller variation in wave velocities. Thus, the variation of elastic properties for ductile iron was not enough to define a linear correlation because all the measurements were practically concentrated in single cluster of points. It is likely that the changes in microstructure between samples from the same pipe are not significant enough to be detected by the ultrasonic velocity measurements. Evaluations of changes in average ultrasonic velocities with average elastic moduli strengths and elongations between pipes were not well correlated as indicated in previous studies performed in controlled laboratory settings although similar trends were observed.

This paper presents novel analysis of ultrasonic measurements using the Fourier and the wavelet transforms. The Fourier analysis was also unable to show good correlations between low strain and large-strain parameters. Lamb waves are typically not considered in the evaluation of ultrasonic pulse velocities. However, Lamb waves were found to contribute significantly to the frequency content of the ultrasonic signals possibly contributing to the poor correlations. The Daubechies's discrete wavelet transform was used in an attempt to isolate p-wave energy with shorter wavelengths and exclude the high-amplitude Lamb wave energy. The resulting analyses showed slight improvements in the correlations between the wave energy (area of the frequency spectra) and large strain measurements, but in general good correlations were still not observed.

Although previous studies available in the literature show good correlations between ultrasonic velocity and tensile strength in grey cast iron and ductile iron; the specimens used in these studies had regular and consistent geometries where changes in microstructure were carefully controlled through manufacturing processes. Conversely, the specimens from exhumed pipes tested in this study varied in cross-sectional area as a result of minor manufacturing defects and different levels of corrosion. These variations impact the large strain testing results but superficial defects have limited effects on wave velocities and may therefore contribute to the low correlations observed

throughout this study. Therefore, correlations between wave velocities and large strain properties obtained using carefully manufactured specimens must be used with caution in the condition assessment of aged water pipes especially for grey cast iron pipes.

Acknowledgements

The authors would like to acknowledge the contribution of the City of Hamilton for providing the pipe samples and the historical records of the pipes; Prof. Tim Topper for thoughtful discussions on the evaluation of the large strain testing; Atif Nazir, Awais Rauf, Douglas Hirst, and Richard Morrison for their help with the experimental program. Our gratitude also goes to Natural Sciences and Engineering Research Council of Canada (NSERC), and the Centre for Advancement of Trenchless Technologies (CATT) at the University of Waterloo for the funding and in-kind contributions for this research.

References

- Abdel-Megeed, S.M. (1984), "Accuracy of correlation coefficient with limited number of points", *J. Exp. Educ.*, **52**(4), 188-191.
- Angus, H.T. (1976), *Cast Iron: Physical and Engineering Properties*, Toronto, Butterworth & Co. Inc.
- ASTM Standard D790 - 07 (2007), *Standard Test Methods for Flexural Properties of Unreinforced and Reinforced Plastics and Electrical Insulating Materials*, ASTM International, West Conshohocken.
- ASTM Standard E8/E8M - 08 (2008), *Standard Methods for Tension Testing of Metallic Materials*. ASTM International, West Conshohocken, PA.
- Bilgin, O. and Stewart, H. (2009), "Pullout resistance characteristics of cast iron pipe", *J. Transport. Eng.*, **135**(10), 730-735.
- Blitz, J. and Simpson, G. (1996), *Ultrasonic Methods of Non-Destructive Testing*, Chapman & Hall, New York.
- Bracewell, R. (2007), *The Fourier Transform and its Applications*, McGraw-Hill, New York.
- Cammarata, M., Rizzo, P., Dutta, D. and Sohn, H. (2010), "Application of principal component analysis and wavelet transform to fatigue crack detection in waveguides", *Smart Struct. Syst.*, **6**(4), 349-362.
- Collins, D. and Alchekh, W. (1995), "Ultrasonic non-destructive evaluation of the matrix structure and the graphite shape in cast iron", *J. Mater. Process. Tech.*, **55**(2), 85-90.
- Davis, J.R. (1996), *Cast Irons*, ASM International, Materials Park, OH.
- Fuller, A., Emerson, P. and Sergeant, G. (1990), "A report on the effect upon mechanical properties of variation in graphite form in irons having varying amounts of ferrite and pearlite in the matrix structure and the use of nondestructive tests in the assessments of mechanical properties of such irons", *AFS Transactions*, **88**, 21-50.
- Graff, K. (1991), *Wave motion in elastic solids*, Dover Publications Inc., New York.
- Gokdag, H. and Kopmaz, O. (2010), "A new structural damage detection index based on analyzing vibration modes by the wavelet transform", *Struct. Eng. Mech.*, **35**(2), 257-260.
- Karsay, S.I. (1970), *Ductile Iron II Engineering Design Properties Applications*, Quebec Iron and Titanium Corporation, Sorel, QC.
- Khan, Z., Cascante, G. and El Naggar, M.H. (2007), "Measurement of dynamic properties of a cemented sand using ultrasonic waves", *Can. Geotech. J.* (in print)
- Koelble, F.T. (2006), *Cast Iron Soil Pipe Fittings Handbook*, Cast Iron Soil Pipe Institute, Washington, DC.
- Lee, S.Y., Rus, G. and Park, T. (2008), "Quantitative nondestructive evaluation of thin plate structures using the complete frequency information from impact testing", *Struct. Eng. Mech.*, **28**(5), 525-548.
- Lu, Y., Ye, L., Wang, D., Zhou, L. and Cheng, L. (2010), "Piezo-activated guided wave propagation and interaction

- with damage in tubular structures”, *Smart Struct. Syst.*, **6**(7), 835-849.
- Makar, J.M. and Rajani, B. (2000), “Gray cast-iron water pipe metallurgy”, *J. Mat. Civil Eng.*, **12**(3), 245-253.
- Ohide, T., Ohira, G. and Ikawa, K. (1989), “Evaluation of mechanical properties of cast iron by ultrasonic velocity”, *Proceedings of the Physical Metallurgy of Cast Iron IV*, Tokyo, Japan, September.
- Orlowicz, W., Tupaja, M., Mróza, M. and Guzikb, E. (2010), “Evaluation of ductile iron casting material quality using ultrasonic testing”, *J. Mater. Process. Tech.*, **210**(11), 1493-1500.
- Rajani, B. (2000), *Investigation of Grey Cast Iron Water Mains to Develop a Methodology for Estimating Service Life*, American Water Works Association Research Foundation, USA.
- Seica, M.V. and Packer, J.A. (2004), “Mechanical properties and strength of aged cast iron water pipes”, *J. Mat. Civil Eng.*, **16**(1), 69-77.
- Skabo, R. and Jackson, R. (1991), *Nondestructive testing of water mains for physical integrity*, CH2M Hill Technical Report, USA.
- Tamburelli, C. and Quaroni, A. (1975), “Ultrasonic velocity measurement to inspect malleable iron castings”, *Non-Destruct. Test.*, **8**(3), 152-157.
- Walton, C.F. (1971), *Gray and Ductile Iron Casting Handbook*, Gray and Ductile Iron Founders’ Society Inc., Cleveland, OH.
- Yang, Y., Cascante, G. and Polak, M.A. (2009), “Depth detection of surface-breaking cracks in concrete plates using fundamental Lamb modes”, *NDT&E Int.*, **42**(6), 501-512.